ORIGINAL ARTICLE

Optimization of Circular Coil Design for Wireless Power Transfer System in Electric Vehicle Battery Charging Applications

Ravi Kumar Yakala[1] · Sumit Pramanick[1] · Debi Prasad Nayak[1] · Manish Kumar[1]

Abstract

In wireless power transfer (WPT) systems, the design of transmitter and receiver coupling coils plays an important role in power transfer. These coupling coils should be capable of transferring power over a large air gap in the order of 140 mm to 210 mm while providing good tolerance to coil misalignment in electric vehicle application. The coil must be designed considering the interoperability, size, weight of the pad, and coupling between the coils to achieve the maximum efficiency from the system. In this paper, circular coil design optimization for a 3.7 kW Type-1 wireless charger has been done by using 3D-Finite Element Method (FEM) analysis. In this work, the influence of change in vertical offset between the coils and misalignment on the critical design parameters such as coupling, quality factor, and mutual inductance is investigated. The number of turns in the coil and its placement optimization has been done. By taking available ferrite cores as a reference, the effect of different core parameters on the coupling coefficient and weight of the pads has been investigated along with flux shielding. Finally, a 450 mm × 450 mm circular pad design is made for 3.7 kW output power. The measured and simulated results for the different vertical offsets and lateral misalignment is investigated.

Keywords Wireless power · Coil design · FEM · EV battery charger

Introduction

Wireless Power Transfer (WPT) is the transfer of power over a large air gap without any contact between the primary and secondary coils (Tesla 1914). The contactless transfer of power makes WPT reliable and safe. Feasibility of WPT has been enhanced in recent years due to development in power semiconductor technology, yielding semiconductor devices capable of fast switching at higher power level. The WPT is becoming more popular in low power applications, electronic appliances charging, and biomedical implantable devices (Mi 2017; Rothstein and Anderlik 2002). However, the recent intensive research in WPT is extended to medium power applications such as dynamic and static wireless charging of electric vehicles (Gozalvez 2007; Miller et al. 2015; Galigekere et al. 2018; Brecher et al. 2014; Hwang et al. 2017). In electrical vehicle charging, transmitter coil also known as primary charging pad, is placed inside the floor. In contrast, the receiver charging pad is placed in the chassis of the electric vehicle. Generally, these power pads are separated in the order of 140 mm to 210 mm, resulting in weak magnetic coupling between the charging pads. Hence these power pads are called loosely coupled.

In WPT, the magnetically coupled coil arrangement plays a vital role in transferring power over a significant distance. The coil arrangement should be designed considering the interoperability of the charging pads, size, and weight of the pad, coupling between the pads and cost (Covic and Boys 2013; Budhia et al. 2011). The interoperability of the pad can be improved by increasing the pad size. But it's weight limits the size of the pad. For power transfer over a large air gap, the leakage flux is very prominent, which leads to a very low coupling between the power pads. The coupling between the pads can be improved by introducing magnetic cores. The core increases the flux linking between the coils by reducing the reluctance, thus increasing the coupling. Generally, ferrite bars are used as the core (Budhia et al. 2011; Lin et al. 2016). By introducing the core into the coil arrangement, coupling between the coils can be improved, but at the same time weight of the charging pads

✉ Sumit Pramanick
  spramanick@ee.iitd.ac.in

[1] Department of Electrical Engineering, Indian Institute of Technology, Delhi, Hauz Khas, New Delhi 110016, India

also increases. So an optimal core selection should be made based on the change in coupling coefficient per unit volume.

In this paper, the design optimization of a circular coil for a 3.7 kW Type-1 wireless charger is carried out by using 3D-FEM analysis. This paper is organized into seven sections, as follows. In Sect. "Inductive Power Transfer System", the basic working of WPT is explained. In Sect. "Coil design considerations", the coil design considerations of WPT is explained. In Sect. "Design optimization of WPT coils", by taking available core as a reference, the effect of the different core parameters on the design of the circular coil pads for effective coupling between the coils and pad optimization is investigated. The selection of the number of turns required and placement of the coil is optimized by using 3D-FEM analysis. In Sect. "Characterisation of the coil", coil characterization is done experimentally. Finally, in Sect. VI, a comparison between measured and simulated results for the 3.7 kW circular charging pad of size 450 mm × 450 mm for different height adjustment and lateral misalignment is shown.

Inductive Power Transfer System

The inductive power transfer (IPT) is a kind of WPT, works on the principle of mutual induction. The IPT system is made up of two magnetic coupled coils, driven by a primary high-frequency power supply and the high-frequency AC to DC pick-up circuit along with a DC-DC regulator, as shown in Fig. 1.

This paper deals with a Type-1, 3.7 kW wireless charger of Z2 category Schneider et al. (2017). Z2 category is a

Fig. 1 Basic building blocks of inductive power transfer

Z-class given by SAEJ2859 standards, based on the ground clearance of WPT. The supply frequency for power pads is in the order of 81.38 kHz–90 kHz, and the nominal operating frequency is 85 kHz. The primary power supply is generally taken care of by the half-bridge or full-bridge inverter. The power transfer capability of the IPT system depends on the magnetic coupling between the coils (i.e., primary and pick-up). These coils are characterized by the self-inductance of the primary coil (L_P), secondary coil (L_S), mutual inductance (M), and coupling coefficient (k). The coupling coefficient of the coils is defined by $k = M/\sqrt{L_P L_S}$. The power transfer capability of the coil is characterized by the open-circuit voltage $V_{oc} = j\omega M I_P$ and the short circuit current $I_{sc} = V_{oc}/j\omega L_S = (M I_P)/L_S$. Where, I_P is the primary coil current, $\omega = 2\pi f_{sw}$ and f_{sw} is switching frequency. The maximum power transfer capability of the coil without compensation (P_{uc}) is given by the product of the open-circuit voltage and the short circuit current.

$$P_{uc} = V_{oc} \times I_{sc} = \omega \frac{M^2}{L_S} I_P^2 \tag{1}$$

The primary coil is compensated for decreasing the Volt Ampere (VA) rating of the primary power supply, by connecting a series capacitive compensator C_P. Series compensation is provided to enhance the power transfer capability in the secondary by connecting a capacitor C_S in series with the secondary coil, as shown in Fig. 2 (Wang et al. 2005; Zhang et al. 2013). Now the power transfer equation is given by

$$P_{out} = P_{uc} \times Q_L = \omega I_P^2 L_P k^2 Q_L \tag{2}$$

where, load quality factor $Q_L = \frac{\omega L_S}{R_{ac}}$. From Eq. (2), it can be observed that the power transfer capability mainly depends on the coupling coefficient and load quality factor. So, the magnetic coupling coils should be designed to transfer the maximum possible amount of power efficiently. The efficiency of the system is given by

$$\eta = \frac{\Re(Z_r) * R_{ac}}{[R_P + \Re(Z_r)] * [R_S + R_{ac}]} \tag{3}$$

where, R_P is primary winding resistance, R_S is the secondary winding resistance, R_{ac} is the equivalent load resistance and $\Re(Z_r)$ real part of the primary reflected secondary impedance. Maximum efficiency at resonance can be achieved at $\frac{d\eta}{dQ_L} = 0$ i.e., $Q_L \simeq 1/k$ as given in Huang et al. (2016). Hence to achieve the maximum efficiency, the load quality factor (Q_L) and the coupling coefficient (k) should be taken into consideration while designing the coil.
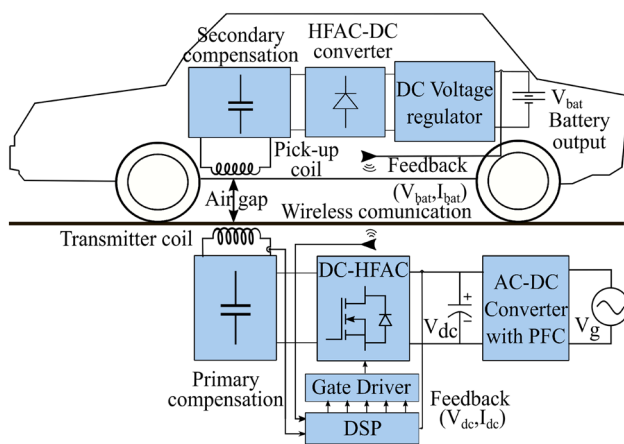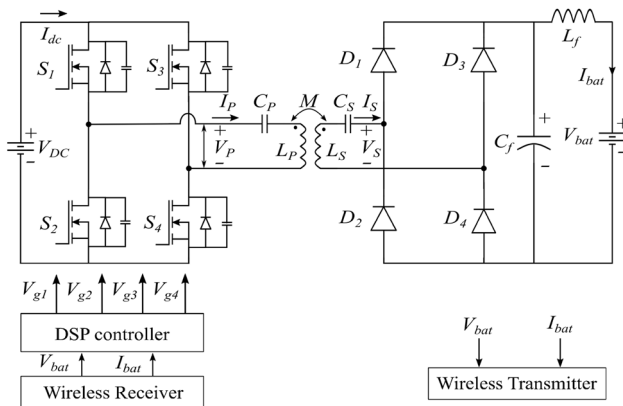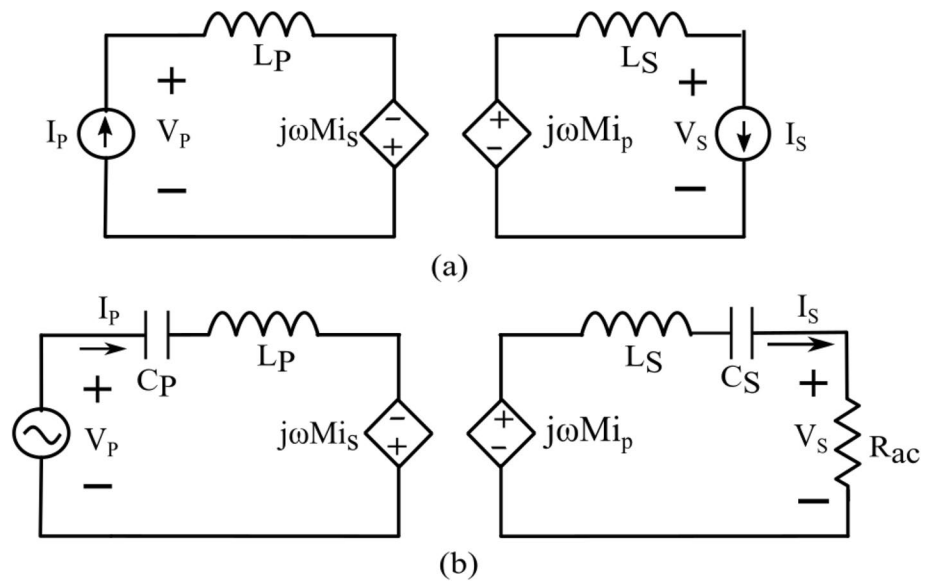
Fig. 2 Equivalent Circuit Model of IPT (**a**) without compensation (**b**) with compensation

Fig. 3 IPT circuit model with series-series compensation

Table 1 Ideal electrical parameters of 3.7 kW charger

Parameter	Value
Output power P_{out}	3.7 kW
Output voltage V_{bat}	136 V
Output current I_{bat}	27.2 A
Primary voltage V_P (rms)	127 V
Primary current I_P (rms)	31.4 A
Primary coil resistance R_P	124 mΩ
Secondary coil resistance R_S	129 mΩ
Peak voltage stress across capacitor V_c (peak)	1265 V
Secondary voltage V_S (rms)	127 V
Secondary current I_S (rms)	30.22 A
Primary self inductance L_P	53.1 (µH)
Secondary self inductance L_S	53.1 (µH)
Mutual inductance M	7.587 (µH)
Coupling coefficient k	0.143

Coil Design Considerations

Electrical Parameters of the 3.7 kW Type-1 Charger

The IPT circuit model with series-series compensation for a 3.7 kW Type-1 charger is shown in Fig. 3 and the electrical parameters for this system are taken as follows. The output battery voltage (V_{bat}) is 136 V, switching frequency (f_{sw}) of 85 kHz and the load quality factor (Q_L) of 7 is selected (Wang et al. 2005; Covic and Boys 2013). To achieve the maximum efficiency at $Q_L = 7$, the nominal coupling coefficient requirement is 0.143. Other electrical and circuit parameters to achieve maximum efficiency are given in Table 1.

Since the operating frequency is of the order of 85 kHz, the losses in the winding caused due to the skin and proximity effects at high frequency should be considered. For

mitigating these effects, generally, Litz wire is used in the design of coil windings. A Litz wire is made up of multiple strands of thin wires to reduce losses caused due to skin and proximity effects.

To reduce these losses, the diameter of the sub-conductor must be less than twice the skin depth $d_{std} < 2\delta$. Where skin depth δ is given by

$$\delta = \sqrt{\frac{\rho_{cu}}{\pi f_{sw} \mu_0}} \qquad (4)$$

where, ρ_{cu} is the resistivity of copper (1.72×10^{-8} Ω.m at room temperature), f_{sw} is the frequency of operation (85 kHz) and μ_0 is the permeability of free space ($4\pi \times 10^{-7}$ H/m). The skin depth of the copper conductor

at an operating frequency 85 kHz is $\delta = 0.2264$ mm, hence we have to select a copper strand of diameter less than 0.4528 mm should be used. In this work, a Litz wire of 784/40 SWG with sub conductor diameter $d_{std} = 0.122$ mm and an overall diameter of the wire at 4.75 mm is chosen for coupling coils design (Parashar vidyut udyog 2019).

Inductance Estimation

Self inductance of a single-layer spiral shown in Fig. 4 is given by Wheeler (1928).

$$L_P = \frac{a^2 N_p^2}{8a + 11c} \quad \mu H \tag{5}$$

where, central radius of the coil $a = R_p + \frac{N_P}{2}(W_p + S_p)$ and width of the coil $c = N_P(W_p + S_p)$. The Eq. (5) gives an error of upto 5% for $a > c > 0.2a$, but it may deviate more if the number of the turns is very less and spacing between the turns is high. The mutual inductance between two non-coaxial filamentary circular coils with parallel axes as shown in Fig. 4, in terms of complete elliptical integrals is given by (Akyel et al. 2009; Raju et al. 2013; Aditya 2018)
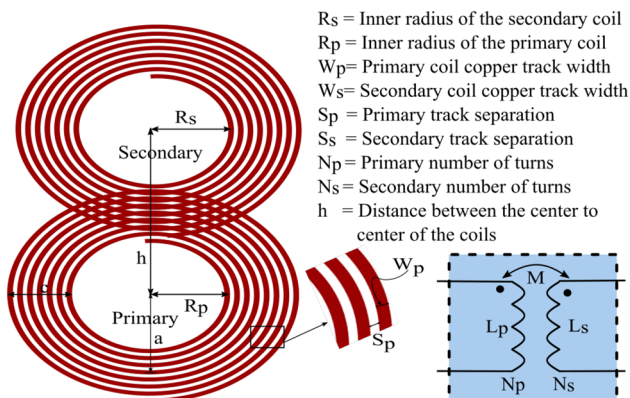
$$M = \sum_{p=1}^{N_p} \sum_{s=1}^{N_s} \frac{2\mu_0 \sqrt{R_p R_s}}{k_{ps}} \left\{ \left(1 - \frac{k_{ps}^2}{2}\right) K_{ps}(k) - E_{ps}(k) \right\} \tag{6}$$

where

$$\alpha = \frac{R_s}{R_p} \quad \beta = \frac{h}{R_p} \quad k_{ps}^2 = \frac{4\alpha}{(1+\alpha)^2 + \beta^2} \tag{7}$$

$K_{ps}(k)$- Complete elliptical integral of first kind.
$E_{ps}(k)$- Complete elliptic integral of the second kind.

Table 2 Coil Parameters Without Core

Parameter	Theoretically	Simulated
	Calculated	In FEM
Self inductance L_P (μH)	36.821	36.921
Mutual inductance M (μH)	3.831	3.617
Coupling Coefficient k	0.104	0.098

By using $R_p = 92.5$ mm, $N_P = 10$, $W_p = 4.75$ mm and $S_p = 0.4$ mm in Eqs. (5) and (6), the self and mutual inductances are analytically calculated. These values are compared with the Ansys Maxwell 3-D FEM simulation and tabulated in Table 2. It is clear that the analytical values are very close to the simulated values.

Design Optimization of WPT Coils

Ferrite Volume Optimization

Coreless coils are ineffective for high power transfer over a large air gap, like EV applications. To increase the power transfer capability and for shaping the flux, i.e., to guide the flux towards the secondary pad, ferrite bars are used. Hence the ferrite bars improve the coupling and reduce energy loss due to the leakage in the magnetic field. But usage of the ferrite bars leads to the hysteresis and Eddy current losses, and also extra ferrite bars lead to the increase in weight of the power pads. Hence an optimization needs to be done in designing the IPT power pads along with the ferrite bars, such that the highest power transfer capability to be achieved for a lesser cubic area of the ferrite bars.

**Fig. 4** Primary and secondary coil interface of wireless power transfer

RS = Inner radius of the secondary coil
Rp = Inner radius of the primary coil
Wp= Primary coil copper track width
Ws= Secondary coil copper track width
Sp = Primary track separation
Ss = Secondary track separation
Np = Primary number of turns
Ns = Secondary number of turns
h = Distance between the center to center of the coils

Fig. 5 3-D FEM simulation of the core showing the flux density distribution in the core of dimensions 186 mm × 27 mm × 16 mm

In ferrite selection, readily available 'I' core with dimensions 186 mm × 27 mm × 16 mm of CF139 grade ferrite is selected. These ferrite bars having a peak flux density of 460 mT and a relative permeability of 2100. From Fig. 5, it can be observed that the peak flux density of the core is around 55 mT at 45 A, 85 kHz supply. Hence it is clear that the core is far away from the saturation limit, which enables better pad design. In the volumetric comparison, the above core is taken as reference, and the length, width, and thickness are varied using Ansys Maxwell 3-D FEM simulation, as shown in Fig. 6. Here the variables are varied from its minimum possible value to maximum value according to the pad dimension of 450 mm × 450 mm. In the Fig. 6 blue curve indicates effect of coupling coefficient with change in width of the core from 10 to 30 mm keeping the length 186 mm and the thickness of the core 16 mm.The orange curve represents effect of the coupling coefficient with change in the core thickness from 6 to 18 mm by keeping the core length 186 mm and the core width 27 mm. And the green curve represents the change in coupling coefficient with respect to change in the length of the core from 150 to 190 mm, keeping the core thickness 16 mm and core width 27 mm.

It is observed that all the curves meet at the reference core design. From Fig. 6, it can be inferred that the effective ferrite utilization per cubic centimeter was substantially high, with an increase in the length of the ferrite bars. This is because the longer ferrite bars provide the highest flux path. Whereas the change in thickness does not have predominant influence on ferrite utilization. So, while considering pad weight, thinner bars are preferred. In this work a ferrite bars of thickness 16 mm are used.
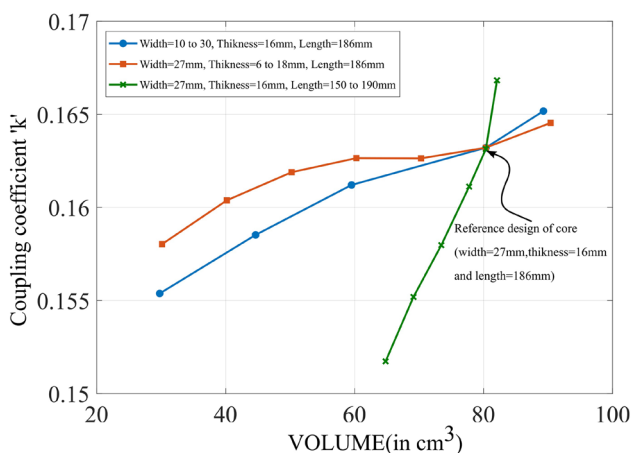
Fig. 6 Volumetric comparison of the coupling coefficient with respect to the core parameters

Coil Placement and the Number of Turns Optimization

The coil placement and the number of turns selection optimization have an impact on the pad weight, losses, and cost. The coil should be placed on the core in an appropriate position such that less copper is required. The increase in copper utilization leads to an increase in copper losses and weight. In this work, for a pad size of 450 mm × 450 mm, the core placement is fixed first with an internal core diameter $C_{in} = 80$ mm and the core length of $C_L = 186$ mm and a Litz wire of diameter $W_p = 4.75$ mm is selected for the winding. Now for a different number of turns, the self-inductance and coupling are observed by changing the coil center diameter. The coil center diameter is $D_{cd} = (D_{in} + D_{out})/2$ where, D_{in} is the inner radius of the coil, $D_{out} = D_{in} + N_P(W_p + S_p)$ is the outer diameter of the coil, S_p is the spacing between the turns and N_P is the number of turns in the primary winding. The number of turns in secondary is equal to the primary number of turns, i.e., $N_S = N_P = N$.

### Optimization of Number of Turns of the Coil for Particular Self Inductance

For a different number of turns, as the central coil diameter increases, the length of the Litz wire required increases. The increase in the length of wire leads to an increase in the copper requirement, which also increases copper losses. By changing the coil diameter for the different number of turns, the self-inductance versus length of wire is plotted, as shown in Fig. 7. From the figure, it is evident that for a given value of self-inductance as the number of turns decreases, the coil diameter provided should increase, which leads to an increase in the length of the wire required. The length of the wire of a spiral coil is given by

$$l = \frac{\pi N_P D_{cd}}{1000} m \qquad (8)$$

As an example, for a particular self-inductance of the coil $L_P = 56.04\ \mu H$, by taking the number of turns in the winding $N = 10$ as a reference, for $N = 13$ requires less length of wire, i.e., from point a to point b is $\Delta l_1 = 0.27$ m of 4% decrements in the length of the wire. Whereas, for $N = 8$ requires more length of wire, i.e., from point b to point c is $\Delta l_2 = 1$ m, which is almost 13.57% increment in length of the wire, as shown in Fig. 7.

The second factor to be considered is the coupling between the coils. By changing the coil diameter for the different number of turns, the coupling coefficient versus length of wire is plotted, as shown in Fig. 8. From the figure, it is clear that as the number of turns decreases the coil diameter
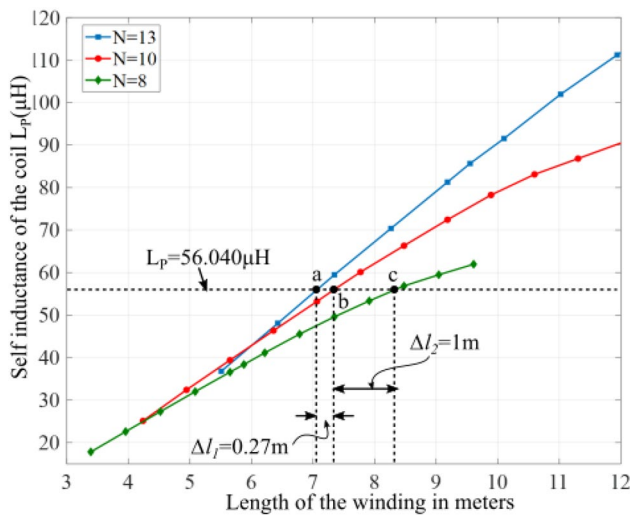
Fig. 7 Change in self inductance with length of the wire as the central diameter of the coil changes
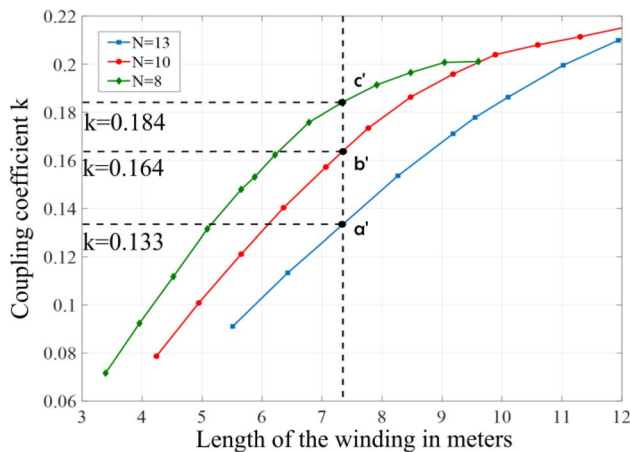
Fig. 8 Change in coupling coefficient with length of the wire as the central diameter of the coil changes

increases and the coupling coefficient k increases from point b' ($k = 0.164$) to a' ($k = 0.184$). Whereas the number of turns increases from 10 to 13 leads to a decrease in the coil diameter. So that the coupling coefficient decreases from the point b' ($k = 0.164$) to the point c' ($k = 0.133$).

Hence it can be concluded that for a given self-inductance, as the number of turns decreases, the copper requirement increases. As the number of turns is increased, it leads to a decrease in the coupling coefficient, so we have to select an optimum number of turns such that copper requirement and coupling coefficient are optimized for a required inductance. Here in this paper number of turns, $N = 10$ is selected for the self-inductance $L_P = 56.04\,\mu H$. The inductance selected is slightly higher than the ideal inductance required, accounting for an error that is expected between the simulated value and practical value.

Coil Placement Optimization

Now another challenge is the placement of the coil on the ferrite core. In the targeted $450\,mm \times 450\,mm$ charging pad, the coil central diameter sweep has been done to select the position of the coil using Ansys Maxwell 3-D FEM tool. The possible minimum diameter of the coil is 135 mm, and the maximum diameter of the coil is 383 mm. In Fig. 9 change of the coupling coefficient per length versus change in the center diameter of the coil is given. From the figure, it is evident that the coupling coefficient per length increases first, then it decreases as the coil diameter increases. So the coil diameter that is chosen is the point where the coupling coefficient per unit length is maximum; here for 10 turns, coil diameter is selected as $D_{cd} = 234\,mm$, which is 52% of the whole pad dimension. The complete design of the coil is done using the Ansys Maxwell 3-D FEM tool, shown in Fig. 10.

Aluminium Backplate

According to the International Commission on Non-Ionisation Radiation Protection(ICNIRP) guidelines 2010 Non-Ionizing Radiation Protection et al. (2010), the electromagnetic fields exposure to the general public and occupational exposure B-field reference levels are given as $27\,\mu T$ and $100\,\mu T$. Hence to reduce the Electromagnetic adverse effect on the human body, proper shielding must be provided. The core material acts as the primary shielding of the magnetic flux. Whereas, aluminum backing is provided as an extra shielding. The aluminum backing plate is also used as a casing for the complete coil structure and acts as a heat sink for
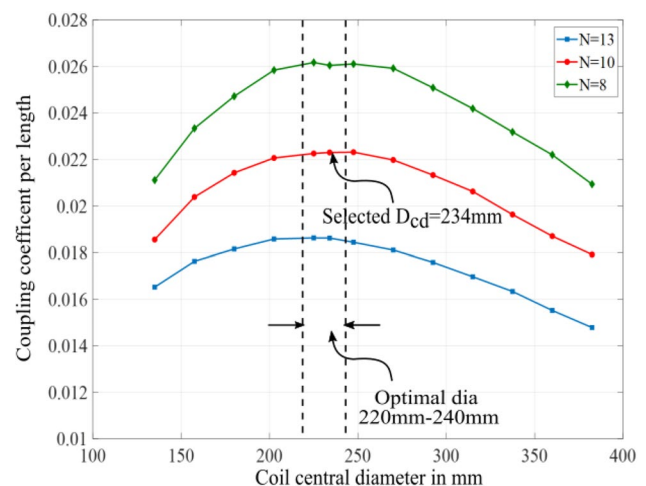
Fig. 9 Change in coupling coefficient per length with the change in central diameter of the coil
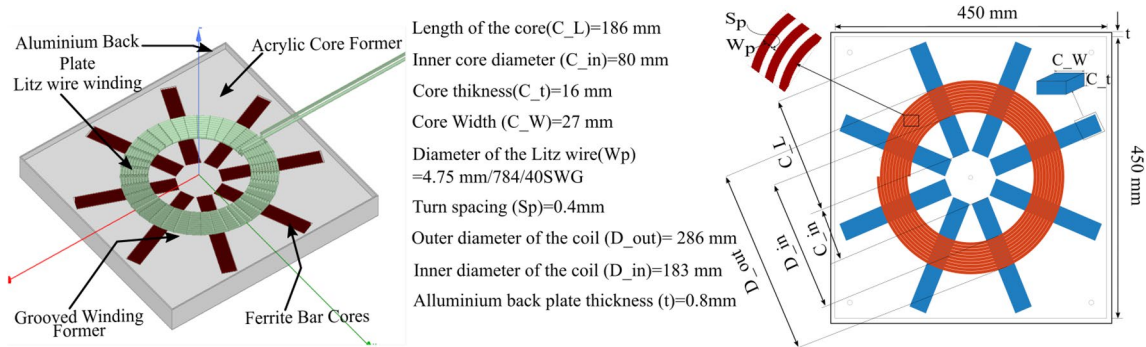
Fig. 10 Schematic of Circular charging pad layout for IPT and dimensions

losses. An Aluminium sheet of thickness 0.8 mm is used in this work for extra shielding. The final designed charging coil pad is shown in Fig. 11. In this design, the cores and the windings are placed in acrylic former with high temperature withstand capability.

Comparative Analysis of the Different Coil Structures with Circular

The advantages of Circular coil over other coil structures such as Double Decouple (DD) coil and Double Decouple Quadrature (DDQ) coil are highlighted below:

– The circular coil constructions are simple and can be easily validated compared to DD and DDQ coils.
– Flux leakage of the circular coil is less, hence high utilization of the winding. Whereas in DD and DDQ coils, the flux pipe is concentrated at centre and very less at the extremes of the coils due to out of phase current passing through the two side by side coils. This leading to more

leakage at the extreme positions of the transmitter coil, hence less copper had been utilised.
– In circular coil the flux distribution is uniform along the axis of the coil, leading to symmetrical tolerance to misalignment between transmitter and receiver coils in all directions. Whereas in other coils like DD and DDQ the flux distribution is not symmetrical in all directions.

A comparative analysis has been done through Ansys Maxwell 3-D FEM simulation studies of different coil configurations to achieve similar self-inductance. The results of the analysis are provided in the Table 3. From above comparison it can be seen that to achieve the required self lesser copper is required in circular coils than DD and DDQ type of coils.

Characterisation of the Coil

For finding characteristics of the coil, i.e., the self and mutual inductance of the coil, a high-frequency square wave is passed through the primary coil while the secondary is left open-circuited as shown in Fig. 12. The primary square wave supply is generated using a full-bridge inverter by providing a 180^0 phase shift between the two legs, and the gating pulses for the inverter are generated using a TMS320F28379D micro-controller. The primary voltage is V_P, self-inductance of the primary coil is L_p, and the primary current passing through the coil is I_P. The self-inductance of the coil calculated for primary as

$$V_P = L_P \frac{dI_P}{dt}$$
$$L_p = \frac{V_P}{dI_P/dt} \tag{9}$$

The primary supply voltage V_P, and primary current I_P are shown in Fig. 13. Similarly inductance of the secondary coil also can be calculated.
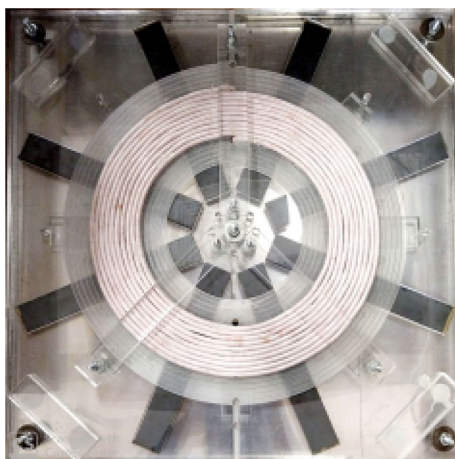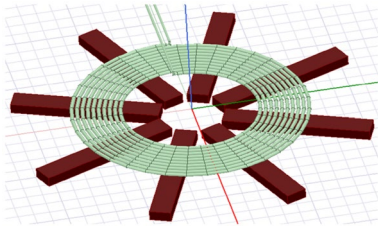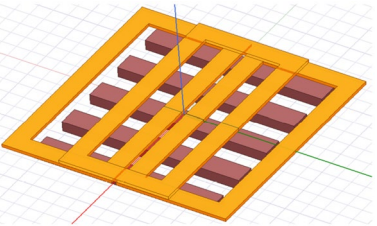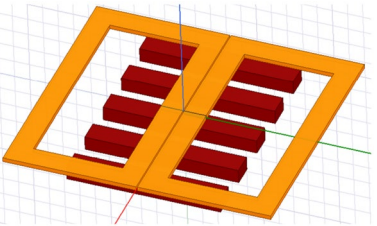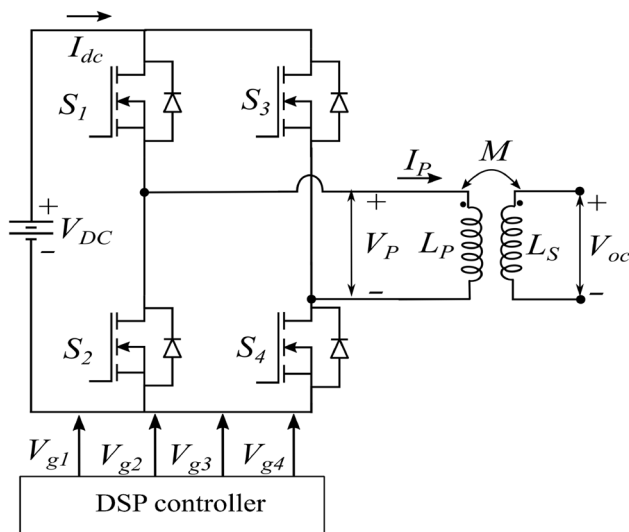

Fig. 11 Designed circular pad layout with 8 ferrite bars and 10 turns

Table 3 A comparative analysis of the different coils, for same dimension of the coil structure by using 3-D FEM analysis

Parameter	Circular coil	DDQ coil	DD coil
Coil structure			
Number of turns per complete coil(N)	10	15	12
(primary or secondary)		(number of turns/coil = 5)	(number of turns per coil = 6)
Self-inductance of the coil (L_P)	50.83 (μH)	50.838 (μH)	50.22 (μH)
Coupling coefficient k	0.151	0.0984	0.1292
Length of the copper wire used (l)	6.822 m	9.150 m	10.2 m
Ferrite volume (V)	642.816 cm^3	907.20 cm^3	432.0 cm^3
Misalignment condition (x)	0 mm	0 mm	0 mm

Fig. 12 Experimental set-up for the measuring the self and mutual inductance
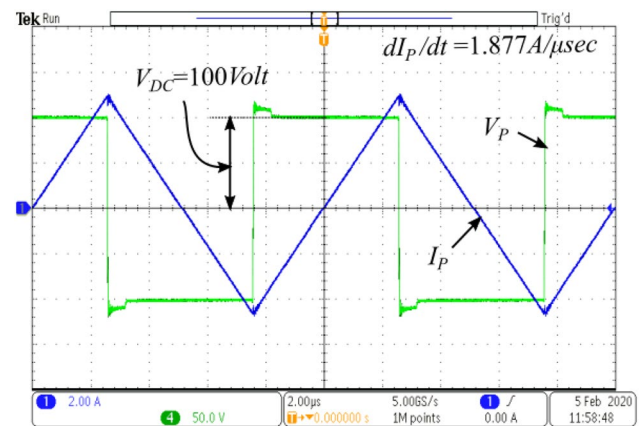
Fig. 13 Voltage across the primary coil and current passing through it when secondary is open circuited. Scale: $V_P \Rightarrow 50\,V/div, I_P \Rightarrow 2\,A/div$, Time $\Rightarrow 2\,\mu\,sec/div$

The mutual inductance of the coupled coils is calculated from open circuit voltage V_{oc} across the secondary terminal and is given by

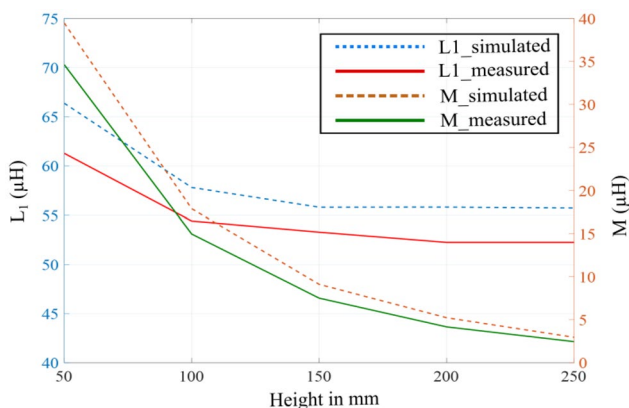$$V_{oc} = M \frac{dI_P}{dt}$$
$$M = \frac{V_{oc}}{dI_P/dt}$$

(10)

Experimental Results and Discussion

To characterize the coil parameters, a DC voltage of 100 V is provided as input to the full-bridge inverter, which generates a square wave of the peak amplitude of 100 V. The characterization of the coil has been done by changing the vertical offset and horizontal misalignment of the coil.

Vertical Offset

The coil parameters are calculated by changing the vertical offset from 50 to 250 mm, keeping both coils are completely aligned. The measured and simulated values of the self-inductance and mutual inductance of the coil by changing the vertical offset are plotted, as shown in Fig. 14. The error in self-inductance measurement is around 6%, and the error in mutual inductance measurement is around 13%. It can be observed that as the vertical offset is changed from 50 to 150 mm, the self-inductance of the coil is reduced by 13% (61.27 μH to 53.277 μH). Whereas from 150 to 250 mm, it is 1.9% (53.277 μH to 52.242 μH), as shown in Fig. 14, which is expected because at lower offset the transmitter and receiver coils are strongly coupled hence the change in the inductance is more. When coils are loosely coupled, the effect of change in offset on the self-inductance of the coil

is almost negligible. But the mutual inductance is decreased from 34.62 μH to 7.51 μH, i.e., drops to 21.7%, as the vertical offset changed from 50 to 150 mm. In contrast, when the vertical offset changed from 150 to 250 mm, it is decreased from 7.51 μH to 2.454 μH, i.e., drops to 32.67%. It is clear that the percentage decrement in the mutual inductance is decreasing as the vertical offset increases.

Horizontal Misalignment

The characterization of the coil is studied by changing the horizontal misalignment from 0 to 200 mm, keeping the vertical offset of 150 mm. The error between the measured and simulated value of self and mutual inductances is 6% and 17%, respectively. The variation in the self and mutual inductance of the coil up to a horizontal misalignment of 50 mm is very less. After 50 mm horizontal misalignment, there is a steep decrease in the mutual inductances, but the change in self-inductance is almost negligible, as shown in Fig. 15. This is
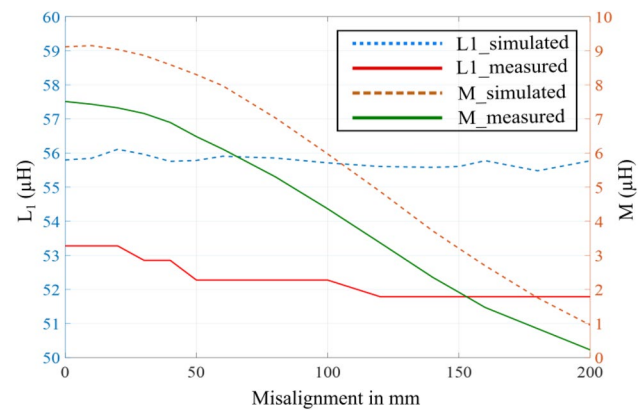
Fig. 15 Measured and simulated self and mutual inductance versus the horizontal misalignment at 150 mm separation

Fig. 14 Measured and simulated self and mutual inductance versus the vertical height offset at 0 mm misalignment
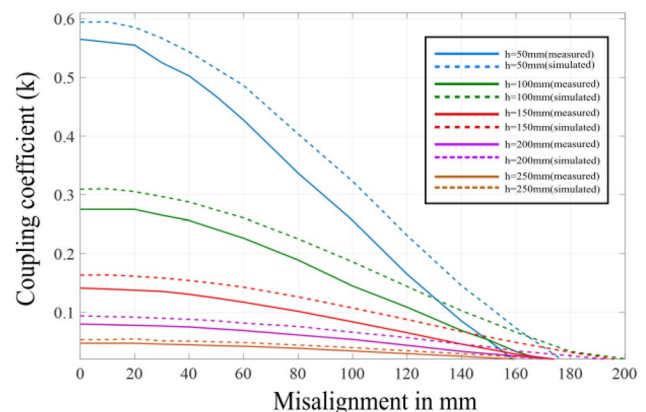
Fig. 16 Measured and simulated coupling coefficient versus the horizontal and vertical offset for 3.7 kW wireless charger of charging pad size 450 mm × 450 mm

because of the loose magnetic coupling between transmitter and pick-up coils due to the horizontal misalignment.

The measured and simulated values of the coupling coefficient(k) profile for different vertical offsets by changing the horizontal misalignment is shown in Fig. 16. The coupling coefficient determines the power transfer capability of the pad from Eq. (2). From Fig. 16, it is evident that as the vertical offset increases, the coupling coefficient decreases, but the decrease in coupling from 50 to 150 mm is comparatively very high than from 150 to 250 mm. The change in the coupling coefficient for the misalignment of 50 mm is almost negligible. Beyond this point up to 160 mm, there a substantial decrement in the coupling coefficient. Irrespective of the vertical offset, the null position is achieved more or less after 160 mm, i.e., 35% of the total pad size. Hence this pad is providing a full power charging zone of 100 mm for the vertical offset of 150 mm. Now the Coil-to Coil efficiency of the Coil is given by Schneider et al. (2017)

$$\eta_{max} = \frac{U^2}{\left[1 + \sqrt{1 + U^2}\right]^2} \tag{11}$$

where $U = k\sqrt{QpQs} = 32.064$ is a figure of merit for a wireless power transfer system, coupling coefficient $(k) = 0.143$, Quality factor of the primary coil $(Q_P) = 228.7$, and Quality factor of the secondary coil $(Q_S) = 219.83$. The estimated efficiency of the designed coil from the Eq. (11) is 93.95%.

Conclusion

The pad design optimization makes the IPT systems more efficient, light, and cost-effective. To achieve the desired coupling between the pads and to achieve the targeted power transfer capability, the ferrite core optimization and coil structure and placement optimization need to be done. In this work, a systematic power pad optimization by using Ansys Maxwell 3-D FEM simulation has been discussed. In this pad design, the flux shielding had been achieved to meet the ICNIRP guidelines using aluminum shielding as casing for the pad. The measured and simulated results for the power pad of dimension $450\,\text{mm} \times 450\,\text{mm}$ are compared for different vertical offsets and horizontal misalignments. The designed power pad can transfer the power of 3.7 kW for the charging zone of 100 mm, up to its full power at a vertical offset of 150 mm.

References

Akyel C, Babic SI, Mahmoudi M-M (2009) Mutual inductance calculation for non-coaxial circular air coils with parallel axes. Prog Elecromagn Res 91:287–301

Aditya K (2018) Analytical design of Archimedean spiral coils used in inductive power transfer for electric vehicles application. Electr Engg 100(3):1819–1826

Brecher A, Arthur D et al (2014) "Review and evaluation of wireless power transfer (wpt) for electric transit applications," John A. Tech. Rep, Volpe National Transportation Systems Center (US)

Budhia M, Covic GA, Boys JT (2011) Design and optimization of circular magnetic structures for lumped inductive power transfer systems. IEEE Trans Power Electron 26(11):3096–3108

Covic GA, Boys JT (2013) Modern trends in inductive power transfer for transportation applications. IEEE Trans Emerg Sel Topics Power Electron 1(1):28–41

Gozalvez J (2007) Witricity-the wireless power transfer [mobile radio]. IEEE Veh Technol Mag 2(2):38–44

Galigekere VP, Pries J, Onar OC, Su G.-J, Anwar S, Wiles R, Seiber L, and Wilkins J (2018) Design and implementation of an optimized 100 kw stationary wireless charging system for ev battery recharging. In: Proc. IEEE Energy Convers. Congr. Expo. (ECCE). IEEE, , pp. 3587–3592

Huang Z, Wong S-C, Chi KT (2016) Design of a single-stage inductive-power-transfer converter for efficient ev battery charging. IEEE Trans Veh Technol 66(7):5808–5821

Hwang I, Jang YJ, Ko YD, Lee MS (2017) System optimization for dynamic wireless charging electric vehicles operating in a multiple-route environment. IEEE Trans Intell Transp Syst 19(6):1709–1726

I C. on Non-Ionizing Radiation Protection et al. (2010) "Guidelines for limiting exposure to time-varying electric and magnetic fields (1 hz to 100 khz)," Health phys., vol 99, no 6, pp. 818–836

Lin FY, Covic GA, Boys JT (2016) Leakage flux control of mismatched ipt systems. IEEE Trans Transp Electrification 3(2):474–487

Mi C (2017) High efficiency wireless power transfer for ev charging and other applications. In: Proc. IEEE Energy Convers. Congr. Expo. (ECCE). IEEE, pp. 1–184

Miller JM, Jones PT, Li J-M, Onar OC (2015) Ornl experience and challenges facing dynamic wireless power charging of ev's. IEEE Circ Syst Mag 15(2):40–53

Parashar vidyut udyog, litz wire catalog (2019), [online]. available:https://parasharvidyutudyog.com

Raju S, Wu R, Chan M, Yue CP (2013) Modeling of mutual coupling between planar inductors in wireless power applications. IEEE Trans Power Electron 29(1):481–490

Rothstein MA, Anderlik MR (2002) The abiocor artificial replacement heart: bioengineering meets bioethics. J Cardiothorac Vasc Anesth 16(2):234–239

Schneider J, Kamichi K, Mikat D, utton R, Abdul-Hak M, Minagawa Y, Abeta H, Taha E, Boyer R, Sirota J et al. (2017) "Bench testing validation of wireless power transfer up to 7.7 kw based on sae j2954," SAE Int. J. Passeng. Cars Electron. Electr. Syst., vol 11, no. 07-11-02-0009, pp. 89–108

Tesla N (1914) "Apparatus for transmitting electrical energy." Dec 1 , uS Patent 1,119,732

Wang C-S, Stielau OH, and Covic G (2005) Design considerations for a contactless electric vehicle battery charger

Wheeler HA (1928) Simple inductance formulas for radio coils. Prog Inst Radio Eng 16(10):1398–1400

Zhang W, Wong S-C, Chi KT, Chen Q (2013) Analysis and comparison of secondary series-and parallel-compensated inductive power transfer systems operating for optimal efficiency and load-independent voltage-transfer ratio. IEEE Trans Power Electron 29(6):2979–2990